High-performance back-illuminated $Ge_{0.92}Sn_{0.08}$/Ge multiple-quantum-well photodetector on Si platform for SWIR Detection

Shaoteng Wu, Shengqiang Xu, Hao Zhou, Yuhao Jin, Qimiao Chen, Yi-Chiau Huang, Lin Zhang, Xiao Gong, Chuan Seng Tan, *Senior Member, IEEE*

***Abstract*—Recently, high-performance GeSn photodiodes with external light illuminated on the device top surface have been demonstrated on various platforms. However, for image sensing systems with a focal-plane array (FPA), the front-illuminated sensors usually suffer from area limitations. Here, we report high-performance back-illuminated $Ge_{0.92}Sn_{0.08}$/Ge multiple-quantum-well (MQW) *p-i-n* photodiode on 300-mm silicon substrate, which was realized entirely by complementary metal-oxide-semiconductor (CMOS) compatible processes. A broadband photo response between 1,000-2,200 nm was observed, and the responsivity is 0.2850 and 0.0085A/W at 1,550 and 2,000 nm, respectively. A specific detectivity larger than 10^9 cm·Hz$^{1/2}$/W was achieved between 1,050 and 1,900 nm, covering all the conventional telecommunication bands (O to U band). Furthermore, the influence of the anti-reflective layers also was studied in detail. The result shows the black Si surface enhances more photo current between 1,000-1,500 nm while the SiO_2 layer (400-nm-thickness) increases more current beyond 1,500 nm. The 3-dB bandwidth was calculated to be up to 8 GHz for a mesa with a diameter of 20 μm at -2 V. Our experiments demonstrated the high-detectivity and high-speed back-illuminated GeSn/Ge MQW photodiode with the potential applications in image sensing systems operated in the short-wave infrared (SWIR) range.**

***Index Terms*—silicon photonics, Infrared detectors, Germanium tin, Black silicon.**

I. Introduction

GESN alloy has drawn much attention recently due to its enhanced carrier mobility, tunable bandgap width, and compatibility with the CMOS processes. GeSn technology has been used to create a plethora of optoelectronic components, ranging from passive devices (multiplexer, waveguide, etc.) to active devices (detector, LED, laser, etc.) [1-6]. Hence, GeSn is a promising group-IV material for infrared imaging sensors by monolithically integrating CMOS read-out circuits with GeSn detectors. Recently, high-performance GeSn photodiodes with external light illuminated on the device top surface (front-illuminated) have been demonstrated on Si, Ge, and Si-on-insulator platforms [7-12]. However, for image sensing systems with a FPA, the front-illuminated sensors usually suffer from area limitations due to the co-located electronic circuits for signal processing. Besides, the metal contacts reduce the effective open area and reflect the incoming light. Thus, for imaging/sensing, the high-performance back-illuminated photodetectors (PDs) with the light signal illuminated on the device's backside are required. Yet, there are only a few reports on back-illuminated GeSn photodiodes [13-15]. The previous back-illuminated GeSn photodiodes from Richard *et al*. show one order of magnitude less responsivity than the front-illuminated device and/or with a narrow spectra response between 1,600 and 1,900 nm due to the absorption from the Ge substrate and its simplified structure design [13, 14].

Thus, back-illuminated GeSn PD on Ge substrate needs to be back-thinned to a thickness of only a few microns or hundreds of nanometers to reduce absorption losses between 1,100-1,600 nm. To overcome this drawback, Si substrates are used for SWIR PDs, which are transparent in the infrared range. Additionally, Si substrates have the following advantages over Ge substrates for short- SWIR PDs: 1) The mature Si microelectronics technology is beneficial to the realization of FPA circuits; 2) Si is one of the most commonly used substrates for growing the high-quality GeSn layer [16-18]; 3) As demonstrated by reported backside Ge PDs, it is easy to use black Si technology to enhance the quantum efficiency of PDs due to the enhancement of light absorption by black Si [19, 20].

In this work, we report the backside-illuminated GeSn/Ge MQW *p-i-n* photodiodes which were grown on the Si substrate. The dark current density (J_{dark}) is as low as ~ 43.2 mA/cm^2 for a reserve bias at -1 V. A broadband photo-response between

This work was supported by the National Research Foundation, Singapore, under its Competitive Research Program (CRP Award NRF-CRP19-2017-01), and Ministry of Education Tier-1 Project under Grant 2019-T1-002-040 (RG147/19 (S)). (*Corresponding author: Xiao Gong and Chuan Seng Tan*)

Shaoteng Wu, Hao Zhou, Yuhao Jin, Qimiao Chen, Lin Zhang, and Chuanseng Tan is with the School of Electrical and Electronic Engineering, Nanyang Technological University, 50 Nanyang Avenue, 639798 Singapore, Singapore (e-mail: shaoteng.wu@ntu.edu.sg; HAO003@e.ntu.edu.sg; YUHAO002@e.ntu.edu.sg; chenqm@ntu.edu.sg; zhang.lin@ntu.edu.sg; TanCS@ntu.edu.sg).

Shengqiang Xu and Xiao Gong is with the Department of Electrical and Computer Engineering, National University of Singapore, 117576 Singapore (e-mail: xushengqiang@u.nus.edu; elegong@nus.edu.sg).

Yi-Chiau Huang is with Applied Materials Inc., Sunnyvale, California, United States (e-mail: yi-chiau_huang@amat.com).

1,000 and 2,200 nm was observed with the responsivity of 0.2850 and 0.0085 A/W at 1,550 and 2,000 nm, respectively. The PDs have a high specific detectivity of > 10^9 cm·Hz$^{1/2}$/W between 1,200 and 1,900 nm, with the detectivity of 7.8*10^9 cm·Hz$^{1/2}$/W at 1550 nm. A novel black Si method also is introduced to enhance light absorption. This study demonstrates the feasibility of the back-illuminated GeSn-based PD for the SWIR image sensing systems.

II. Device Design and Measurement

The GeSn/Ge MQW sample was grown on a double-sided polished Si substrate (300 mm) using an industry-standard reduced pressure chemical vapor deposition (RPCVD) system with GeH_4 and $SnCl_4$ as Ge and Sn precursors, respectively. For the initial growth stage, a ~1,500 nm of strain-relaxed Ge buffer layer was grown to confine the defects near the interface of Ge/Si. *In-situ* doping was used to develop the p-type (boron as dopant) and n-type (arsenic as the dopant) Ge contact layers. Between these two contact layers, the 15 periods of intrinsic GeSn/Ge MQW with 7.5 nm of $Ge_{0.92}Sn_{0.08}$ well layer and 20 nm of Ge barrier layer was grown. Fig. 1(a) shows the typical symmetric XRD ω-2θ scan of the MQW from the (004) plane. Satellite peaks are observed clearly, indicating the high crystalline quality and uniform thickness of the MQW. The asymmetric (224) reciprocal spacing mapping (RSM) in Fig.1(b) shows the GeSn layers are fully strained in the MQW structure as the GeSn and Ge peaks have the same reciprocal lattice vector along the Q_x direction.

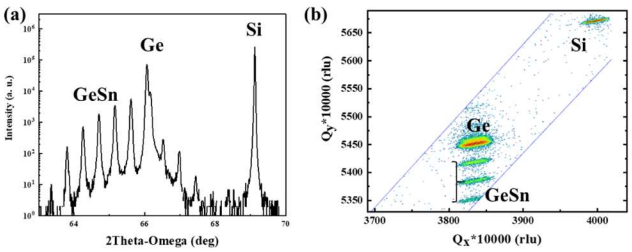

Fig. 1. (a) XRD (004) ω-2θ scan and (b) asymmetric (224) RSM of the GeSn/Ge MQW photodiode.

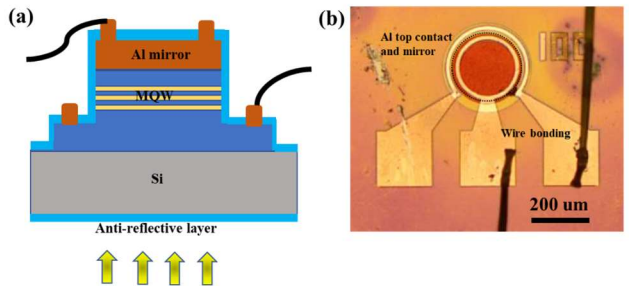

Fig. 2. (a) schematic diagram and (b) optical microscope image of the back-illuminated GeSn/Ge MQW photodiode with wire bonding.

Fig. 2(a) shows the schematic diagram of the back-illuminated GeSn/Ge MQW PD with bonding wires for subsequent electrical measurement. This sample has circular mesas made by standard photolithography and chlorine-based reactive ion etching (RIE). Firstly, circular mesa regions were patterned, followed by the metal mirror (Ti/TiN/Al, 20/50/300 nm) sputtering. Subsequently, the top mesas were formed to expose the p-Ge region by the RIE process using the metal mirror as the hard mask. A second RIE process was performed to form the bottom mesa to make the electrical isolation between each device. After creating the double-mesa structure, plasma-enhanced chemical vapor deposition (PECVD) was used to deposit a 400 nm passivation SiO_2 layer. Finally, electrode pads were deposited with 20/50/300 nm of Ti/TiN/Al. As a reference, the front-illuminated PD was fabricated on the same MQW epitaxial wafer as well. To study the effect of the anti-reflective layers, SiO_2 layer and black Si structure was designed and deposited on the backside of the polished Si surface. This SiO_2 anti-reflective layer was deposited by PECVD with a thickness of ~400 nm. The black Si consisting of high-density nanowires is fabricated by RIE etching of Si. As shown in Fig.2(b), the optical microscope image shows the back-illuminated PD with bonding wires. For the electrical and light response measurements of the back-illuminated GeSn PD, gold wire bonding was used to connect the electrode pads from the chip to the plastic chip carrier with two gold-covered conductors. A hole was made in the chip carrier directly below the device under test to allow the light to propagate into the sample from the backside. The fiber lasers (Tunable 1,500-1,630 nm, Tunable 1,000-2,400 nm, 2,000 nm laser), connected to the Keithley 2450 semiconductor parameter analyzer, were used to measure the current-voltage characteristic of the MQW *p-i-n* PDs.

III. Results and Discussion

A. Dark current analysis

The dark current of the back-illuminated PDs was measured with the mesa diameter between 60 and 250 μm from -1 to 1 V (Fig. 3(a)). For the device diameter of 60 μm, the dark current is 2.08 μA at -1 V, among the lowest of other published GeSn PDs. The high on/off ratio of ~10^4 under 1 V demonstrates the photodiode's excellent rectifying behavior. The 250 μm device has the lowest dark current density (J_{dark}) of ~43.2 mA/cm^2, which is comparable with that of the reported group-IV photodiodes[7, 21, 22]. This low J_{dark} is mainly due to the low bulk leakage current densities (J_{bulk}) from the pseudomorphic MQW layers which have a low-density dislocations. The J_{dark} consists of surface leakage current densities (J_{surf}) and J_{bulk}, which is expressed as: $J_{dark} = J_{bulk} + \frac{4}{D} J_{surf}$. According to this equation, the J_{dark} at a given reverse bias is linear to 4/D. After substituting the value of J_{dark} and its corresponding D, the J_{surf} and J_{bulk} can be calculated from linear interpolation in the scatter plot, which are 35.8 and 54.0 μA/cm, respectively (Fig. 3(b)). The inset in Fig. 3(b) shows the percentages of surface leakage with different mesa diameter. The increased J_{surf} with the decreasing of the mesa diameter is attributed to the increase of the perimeter-to-area ratio. The dark current could be further reduced after optimizing the processes, such as more effective passivation

treatment using amorphous Si or GeO_2 as the passivation layer [23-25].

The dark current of the back-illuminated GeSn PD was further analyzed using the diode current formula:

$$I = I_0 exp\left[\frac{q(V-R_S I_{net})}{nKT}\right] + \frac{V}{R_{Sh}} \quad (1)$$

where I_0, R_S, R_{Sh}, and I_{net} is the reverse saturation current, series resistance, shunt resistance, and net current flow. I_{net} can be calculated by the formula of $I_{net} = I - V/R_{Sh}$. By dV/dI, the shunt resistance can be calculated near 0V. The shunt resistances of the back-illuminated GeSn PD is 30 kΩ for mesa diameter of 250 μm. I_{net} is obtained by substituting the shunt resistance into the above equation. Using the transformed expression: $dV/dI_{net}=(nkT/q)\, I_{net}^{-1}+R_S$, the series resistance is obtained, as shown in Fig. 3c. The series resistance is as low as 10.73 Ω. The high shunt resistance and low series resistance are beneficial to the high specific detectivity and 3-dB bandwidth of the back-illuminated PD, which will be discussed in part D and E.

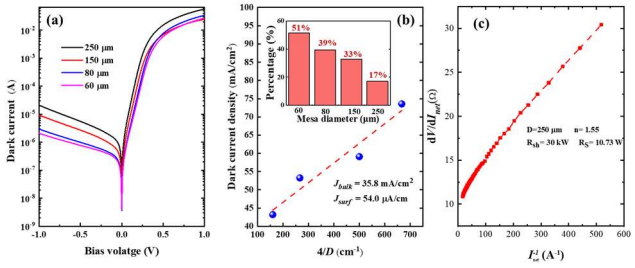

Fig. 3 (a) Current–voltage curve of back-illuminated GeSn/Ge MQW photodiodes with different mesa diameters in a dark environment. (b) The J_{dark}-$4/D$ characteristic at −1 V. Inset (b) shows the surface leakage percentages with varying mesa diameters. (c) Linear interpolation of Inet-1 versus dV/dInet for the back-illuminated GeSn photodiode.

B. *Photo current analysis*

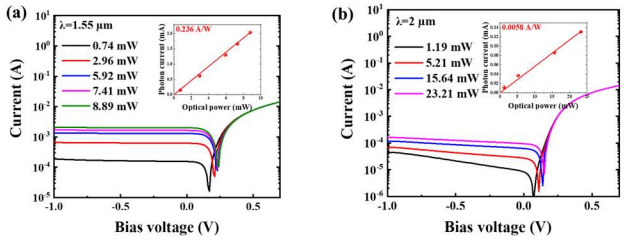

Fig. 4. (a) and (b) Current–voltage curve of the back-illuminated GeSn/Ge MQW photodiodes under 1,550 and 2,000 nm laser with varying optical power. Inset shows the photocurrent as a function of the optical power.

The steady-state photocurrent of the back-illuminated GeSn/Ge MQW devices without an anti-reflective layer was measured for the mesa size of 250 μm. Fig. 4(a) and (b) show the back-illuminated photodiode current-voltage characteristics under 1,550 and 2,000 nm laser with varying optical power. Two optical fiber lasers (2,000 nm, Thorlabs-FPL2000; tunable 1,500-1,630 nm, T100S-HP) were used, and the propagation and coupling loss is calibrated by the standard power meter beforehand. As shown in Fig. 4(a), the photocurrent increases, and no current saturation is observed when the laser power increases from 0.73 to 8.89 mW (1,550 nm). Furthermore, the photo current curves are completely flat from -1 to 0 V, indicating the efficient collection of the photocarriers occur. By linear interpolation between optical power and photocurrent, the back-illuminated GeSn photodiode has a relatively high responsivity ~ 0.236 A/W at 1,550 nm (inset Fig. 4(a)). Similarly, the photodiode's optical response was measured and extrapolated at 2,000 nm, shown in Fig. 4(b). At 2,000 nm, the back-illuminated device has the extracted responsivity of about 0.0058 A/W. The photo current analysis demonstrates that the back-illuminated GeSn/Ge MQW PD has the photodetection capability from 1,550 to 2,000 nm.

C. *Effect of anti-reflective layer*

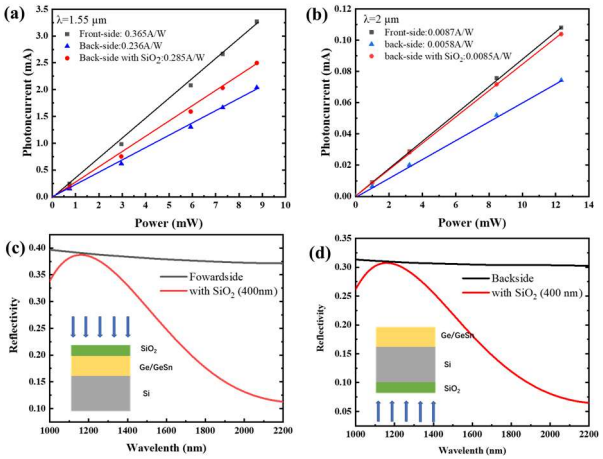

Fig. 5. Photocurrents of the GeSn/Ge MQW photodiodes (Front-side, back-side with and without the SiO_2 anti-reflective layer) at a reverse voltage of 1 V under the illumination at (a) 1,550 nm and (b) 2,000 nm wavelength. FDTD reflectivity simulation of (c) the front- and (d) back-illuminated PDs with or without SiO_2 anti-reflective layer.

Fig.5(a) and (b) show the comparison of photocurrents between the back-illuminated PDs (blue line) and front-illuminated PDs (black line) at different power intensities at 1,550 and 2,000 nm, respectively. The responsivity of the back-illuminated PDs is 64.7% and 66.7% of the front-illuminated PDs at 1,550 and 2,000 nm. In contrast to the front-illuminated devices, no SiO_2 anti-reflection layers were deposited on the light incident window of the back-illuminated PDs. As shown in Fig.5(c), the finite-difference time-domain (FDTD) simulation indicates that the reflectivity decreases from 0.38(0.37) to 0.27 (0.13) at 1,550 (2,000) nm after depositing a 400 nm SiO_2 on the Ge layer for the front-illuminated device. Thus, an absorption enhancement of 17-38% could be speculated in the wavelength range of 1550-2000 nm after depositing SiO_2 layer on the front-illuminated device. For the

back-illuminated photodiodes, a 400 nm SiO_2 layer was deposited on the Si after front side processing. The red lines in Fig.5(a) and (b) shows the responsivity increased to 0.285(0.0087) A/W at 1,550 (2,000) nm. The 21% (47%) enhancement of responsivity at 1,550 (2,000) nm is consist to the 17% (31%) absorption enhancement calculated by the FDTD simulation (Fig.5 (d)). Though the responsivity of the back-illuminated PDs at 2,000 nm is equal to that of the front-illuminated PDs, an obvious difference in the responsivities between back- and front-illuminated PD at 1,550 nm was observed (0.285 A/W versus 0.365A/W). This is due to the high absorption of the thick Ge buffer layer at 1,550 nm. By substituting the absorption coefficient of the Ge (α, 3,241 cm^{-1} at 1,550 nm) and the thickness of the Ge buffer layer (z, ~1,500 nm) to the equation: A(z)=1-exp(-αz), the absorption of the Ge buffer layer at 1,550 nm is ~0.39. The absorption coefficient was obtained from an ellipsometer data of the as-grown Ge-on-Si sample, grown by RPCVD with similar growth conditions. This means an additional 39% light can be absorbed in the MQW at 1,550 nm and contributes to the photocurrent of the PDs.

Furthermore, besides the SiO_2 layer, micro-and nano-structures, such as polarizers, diffraction gratings, antireflection structures, or plasmonic structures can be utilized on the backside to improve the light absorption and quantum efficiency of the PD [19]. One approach is to use stochastic wire-like structures, called black Si. The advantage of black Si over other microstructures is the easy fabrication without requiring lithographic technology and low cost [26, 27]. A boosted responsivity has been demonstrated for the back-illuminated Ge on Si photodiodes using the black Si [20].

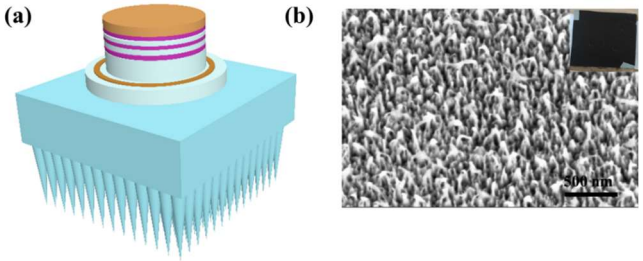

Fig. 6. (a) 3-D schematic of the black Si GeSn/Ge MQW photodiode. (b) SEM image of the nanowire structured black Si fabricated via RIE. The inserted shows the photograph of the black Si.

Fig.6(a) shows the 3-D schematic of the GeSn/Ge MQW photodiode with nanowire-structured black Si on the black side. The black Si surface was achieved after front side processing from a novel RIE etching. For this etching, the device with the Si surface was upside placed on an 8-inch Si carrier which was covered with a 10 nm gold layer deposited by electron beam evaporation. Then, the surface with the nanowires was achieved by RIE etching using Cl_2 plasma gas for 3 minutes. An RF power of 200W, a chamber pressure of 20 mT, and a Cl_2 flow of 50 sccm were utilized. During the etching process, the reactive Cl-based species will react with the Si to form a volatile $SiCl_4$ product which was desorbed from the substrate surface. Meanwhile, the high ion energy Cl-based species will physically bombard the gold surface, resulting in the deposition of gold particles on the Si surface. Due to the shielding effect of gold, the nanowire structure was formed during the continued etching process of Si. We found that this method is efficient, wafer-scale, and can be used to form black germanium as well. The details will be published elsewhere. Fig. 6(b) shows the SEM images of the black Si after the RIE etching. High density, stochastic Si nanowires are perpendicular to the substrate. The inserted photograph shows the black color of the substrate indicating no obvious light reflection.

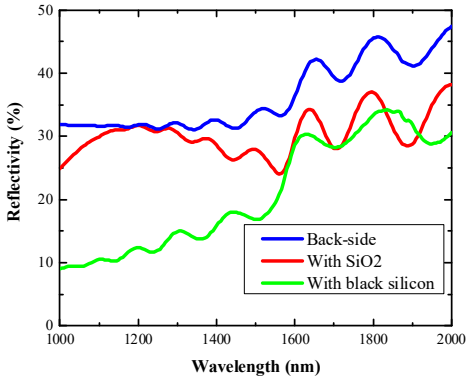

Fig. 7. Reflection spectra of GeSn/Ge MQW epitaxial samples in the wavelength range of 1,000 to 2,000 nm. The light is incident on the back-side (Si-side) and a 20/50/300 nm Ti/TiN/Al was deposited on the front-side (Ge-side).

Fig. 7 shows the reflection spectra of GeSn/Ge MQW epitaxial sample with/without anti-reflective layer (SiO_2 and black Si) with the incident light from the backside in the wavelength range of 1,000 to 2,000 nm. As the spot area of the spectrophotometer (LAMBDA 950) is above 0.5*0.5 cm^2, the choose samples are epilayers, not fabricated devices. The front surfaces of the three samples are covered with the reflective mirror (20/50/300 nm Ti/TiN/Al). Resonance peaks were observed in these reflection spectra due to the cavity structure between metal-Ge and Ge-Si interfaces. It can be observed that the sample with the SiO_2 layer or black Si (red and green line) reflects less light in the whole waveband than that of the regular sample (blue line)). Obviously, the black Si sample reflects less light at a shorter wavelength (1,000-1,550nm). The shorter wavelength, the greater difference between the regular samples was observed. For the nanostructured surface, the broadband antireflection only happens when the height of the nanostructure is > 0.4λ (λ, wavelength) and the domain spacing is < $\lambda/2n_s$ (n_s, refractive index of the substrate)[28]. Thus, the increase of the reflection of the black Si after 1500 nm should be due to the NW's shortness (<1,000 nm). On the contrary, the SiO_2 layer mainly reduces the reflectivity longer than 1400 nm, as proved by the FDTD simulations above.

As shown in Fig. 8, the curves show the optical responsivity spectra of the front- (black line) and back-illuminated GeSn/Ge MQW photodiodes (blue, red, and green line for regular, SiO_2-, black-Si- covered devices, respectively) at -1 V from 1,000 to 2,100 nm wavelength. This measurement was achieved by combining a high-power supercontinuum source (SC-Pro-7,

400 to 2,400 nm) and a laser line tunable filter (Photon, etc. 1,000-2,300 nm). A commercial GaAs PD was used to calibrate the power density. We found the responsivity values using the supercontinuum source is less than the tunable 1,500-1,630 nm laser (~30-40%, Fig. 4 and Fig.5), mainly due to the larger light spot diameter (62.5 μm compared to 10 μm). The back-illuminated GeSn PD has a high responsivity for all the conventional telecommunication bands (O to U band). Consistent with the above analysis, the black Si enhances more photo current between 1,000-1,500 nm while the SiO_2 layer (400-nm-thickness) increase more between 1,500-2100 nm from the regular device. For the SiO_2 covered device, responsivity around 0.2 A/W was achieved for laser wavelength from 1,200 to 1,600 nm. Additionally, a responsivity larger than 0.05 A/W was also observed when the wavelength < 1,880 nm, which shows the extended detection capabilities of PD compared to Ge material. Compared with the front-illuminated device curve, a noticeable value gap appears when the wavelength is less than 1,580 nm, due to the absorption from the Ge buffer layer (1,000-1,600 nm) and Si substrate (1,000-1,150 nm). For the wavelength between 1,580 to 2,200 nm, the responsivity of the SiO_2 covered back-illuminated PD is the same as the front-side one. A further increase of the responsivity could be expected if the back mirror (Ti/TiN/Al) is optimized to single layer Al or Au, as the Ti and TiN layer has a considerable infrared light absorption [29]. However, as shown in Fig. 8, the responsivity and detection range of the back-illuminated GeSn photodiodes in this work is significantly better than the previously reported value [13, 14].

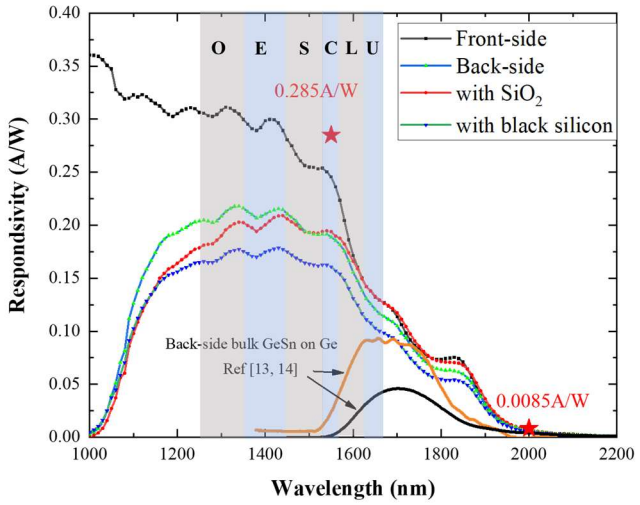

Fig. 8. (a) Optical responsivity curves of GeSn/Ge MQW photodiodes in the wavelength range of 1,000 to 2,200 nm at -1V, compared to the previous back-illuminated GeSn photodiodes.

The responsivity spectra also show the photocurrent decreases rapidly after 1,860 nm with a negligible response after 2,100 nm. The electronic band structure of the GeSn was calculated using the model-solid theory. The energy shifts of the strained GeSn layer was calculated from the deformation potential theory. Here, the used strain for the GeSn layer is -1.16 and 0.88%, along with in-plan and normal directions, respectively, as revealed in the RSM measurement. By calculating 1-D time-independent Schrödinger's equation, the ground states of the conduction band *L*- and *Γ*-valleys, heavy-hole (*HH*), and light-hole (*LH*) bands were obtained. The bandgap analysis shows the direct bandgap of the GeSn well, the difference between the *Γ*-valley electron and heavy hole ($E_{\Gamma 1}$-E_{hh1}) energy, is around 0.658 eV (1884 nm)[30]. This result shows good agreement with the rapid decrease of light detection performance after 1,860 nm.

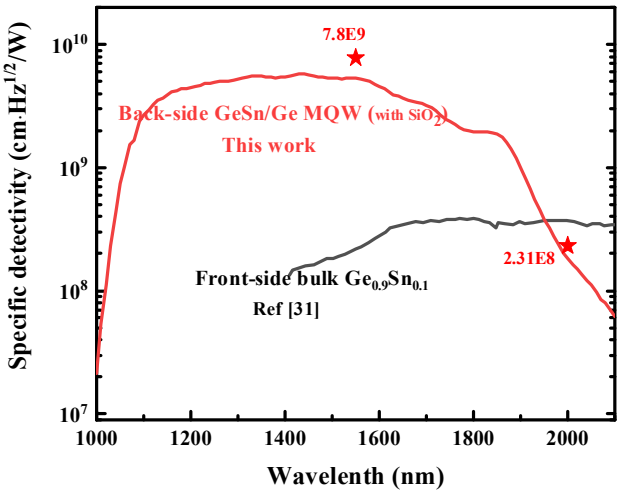

Fig.9. Specific detectivity (D*) of the back-illuminated GeSn/Ge MQW PD without any anti-reflection coating, compared to the previous front-illuminated bulk $Ge_{0.9}Sn_{0.1}$ photodiode.

D. Specific detectivity analysis

Based on the above obtained dark current and responsivity, the specific detectivity *D** of the photodiodes was investigated with the comparison to the previous bulk GeSn photodiodes from Ref [31]. *D** is expressed as $R\frac{\sqrt{A\Delta f}}{\sqrt{I_n^2}}$, where *R, A,* Δf and I_n^2 is the responsivity, active area of the PD, bandwidth and mean squared noise current. Under ideal conditions, the photodiode's noise current generally consists of thermal fluctuations ($I_{Thermal}$) and shot noise (I_{Shot}): $I_n^2 = \sqrt{I_{Therm}^2 + I_{Shot}^2}$. The $I_{Thermal}$ is described as: $I_{Therm} = \sqrt{4kT\Delta f/R_{shunt}}$, where *k, T,* and Δf and is the Boltzmann constant, absolute temperature, and bandwidth, respectively. For the mesa diameters of 250 μm, the R_{shunt} is around 30.0 kΩ. Thus, the $I_{Thermal}$ could be calculated to 7.43×10^{-13} A·Hz$^{-1/2}$ (T=300 K). For I_{Shot} which evaluates the carrier fluctuations are expressed as $I_{Shot} = \sqrt{2q(I_{Dark} + I_{Photo})\Delta f}$. Benefit from the low dark current owing to the pseudomorphic GeSn growth, the shot noise current was calculated to be ~3.12×10^{-13}A·Hz$^{-1/2}$ at -0.01 V by assuming the optical power is close to 0. A high specific detectivity of >10^9 cm·Hz$^{1/2}$/W was achieved between 1,050 and 1,900 nm (Fig. 9). The specific detectivity of back-illuminated MQW GeSn PD is ~7.8×10^9 cm·Hz$^{1/2}$/W at 1,550 nm which is 35 times higher than that of the front-side bulk

$Ge_{0.9}Sn_{0.1}$ PD [31].These results in the higher detectivity of the back-illuminated GeSn PD as compared to the previous work of the front-illuminated structure between the wavelength of 1,400 and 1,900 nm [31]. As discussed above, the dark current and the responsivity could be improved by optimizing the fabrication processes, and eventually increasing the detectivity further.

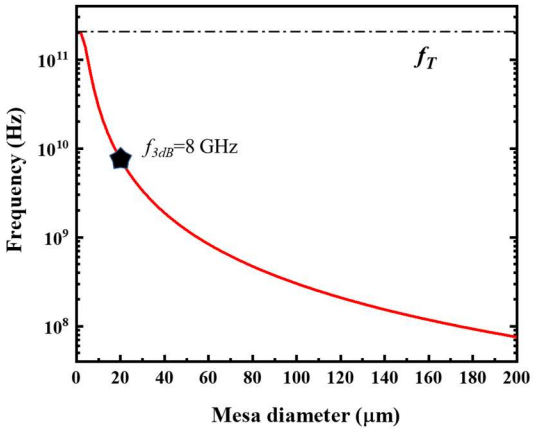

Fig.10. Theoretical 3dB bandwidth of the back-illuminated GeSn/Ge MQW photodiodes at -2V with different mesa diameters.

E. 3-dB bandwidth analysis

Finally, the calculated 3-dB bandwidth of back-illuminated MQW PD was shown in Fig. 10. For the high-frequency response, only the transit-limited bandwidth (f_T) and *RC* delay-limited bandwidth (f_{RC}) has been considered: $f_{3\,dB} = \sqrt{\frac{1}{f_T^{-2}+f_{RC}^{-2}}}$[32]. The transit bandwidth (f_T) was calculated by $f_T = 0.45V_{sat}/d_i$, where d_i is the thickness of the depletion layer and V_{sat} is the saturation velocity which is considered to be 6×10^6 cm/s from Ge material. The *RC* frequency (f_{RC}) is linear to the d_i and inversely proportional to the surface area and it is expressed by $f_{RC} = \frac{1}{2\pi RC}$. *R* consists of series resistance (R_s) and load resistance (R_l=50 Ω). The R_s was calculated ~ 10.73 Ω, as shown in Fig. 3c. *C* consists of junction capacitance C_j and parasitic capacitance C_p, which both were obtained from the capacitance-voltage measurement at dark conditions. The theoretical *3dB* bandwidth of the back-illuminated PD is ~8 GHz (at -2 V) for the mesa diameter of 20 μm (Fig. 11). This theoretical calculation is at the same scale as our previous results on the front-side MQW structure which has a measured 3dB bandwidth of ~2 GHz at -3V with the mesa diameter of 60 μm [7]. The back-illuminated photodiode's calculation bandwidth is slightly overestimated at low bias voltage due to the carrier trapping effect in the MQW. However, the back-illuminated MQW PD presented in this work suggests that it could be operated at high frequency, as the carrier trapping effect would be weakened when the bias voltage is high.

IV. Conclusion

High-performance back-illuminated GeSn/Ge MQW PD was demonstrated on 300 mm Si substrate by CMOS compatible processes. The device has a dark current density of ~ 43.2 mA/cm^2 (at -1V), among the lowest values in the reported group-IV photodiodes. A broadband photo response between 1,200 and 2,100 nm was observed and with the responsivity of 0.285 and 0.0085 A/W at 1,550 and 2,000 nm, respectively, close to the corresponding front-illuminated structure. A high specific detectivity of >10^9 cm·Hz$^{1/2}$/W was achieved between 1,200 and 1,900 nm (covering all the conventional telecommunication bands), which is among the highest value in the reported GeSn photodiodes. Furthermore, the study of the anti-reflective layers shows the black Si surface mainly increases the photocurrents of the PDs between 1,000-1,500 nm while the SiO_2 layer (400-nm-thickness) mainly increases the photocurrents of the PDs between 1,500-2,100 nm. The theoretical *3dB* bandwidth of the back-illuminated PD is ~8 GHz (at -2 V) for the mesa diameter of 20 μm. This high performance back-illuminated GeSn-based MQW photodiode demonstrate the potential applications in the image sensing systems in the SWIR range.

Acknowledgment

The authors would like to thank Nanyang NanoFabrication Centra (N2FC) for the use of semiconductor process equipment.

References

[1] H. Tran *et al.*, "Si-based GeSn photodetectors toward mid-infrared imaging applications," *ACS Photonics,* vol. 6, no. 11, pp. 2807-2815, 2019.

[2] J. Zhou et al., "Ferroelectric Negative Capacitance GeSn PFETs With Sub-20 mV/decade Subthreshold Swing," IEEE Electron Device Letters, vol. 38, no. 8, pp. 1157-1160, 2017

[3] A. Elbaz *et al.*, "Ultra-low-threshold continuous-wave and pulsed lasing in tensile-strained GeSn alloys," *Nature Photonics,* vol. 14, no. 6, pp. 375-382, 2020.

[4] S. Wirths *et al.*, "Lasing in direct-bandgap GeSn alloy grown on Si," *Nature photonics,* vol. 9, no. 2, pp. 88-92, 2015.

[5] M. Oehme et al., "Room-Temperature Electroluminescence From GeSn Light-Emitting Pin Diodes on Si," IEEE Photonics Technology Letters, vol. 23, no. 23, pp. 1751-1753, 2011

[6] H. Cong et al., "Silicon Based GeSn p-i-n Photodetector for SWIR Detection," IEEE Photonics Journal, vol. 8, no. 5, pp. 1-6, 2016.

[7] H. Zhou *et al.*, "High-efficiency GeSn/Ge multiple-quantum-well photodetectors with photon-trapping microstructures operating at 2 μm," *Optics Express,* vol. 28, no. 7, pp. 10280-10293, 2020.

[8] Y.-H. Huang, G.-E. Chang, H. Li, and H. Cheng, "Sn-based waveguide pin photodetector with strained GeSn/Ge multiple-quantum-well active layer," *Optics Letters,* vol. 42, no. 9, pp. 1652-1655, 2017.

[9] G.-E. Chang, R. Basu, B. Mukhopadhyay, and P. K. Basu, "Design and Modeling of GeSn-Based Heterojunction Phototransistors for Communication Applications," IEEE Journal of Selected Topics in Quantum Electronics, vol. 22, no. 6, pp. 425-433, 2016

[10] B.-J. Huang, J.-H. Lin, H. Cheng, and G.-E. Chang, "GeSn resonant-cavity-enhanced photodetectors on silicon-on-insulator platforms," *Optics letters,* vol. 43, no. 6, pp. 1215-1218, 2018.

[11] C.-H. Tsai, B.-J. Huang, R. A. Soref, G. Sun, H. Cheng, and G.-E. Chang, "GeSn resonant-cavity-enhanced photodetectors for efficient photodetection at the 2 μm wavelength band," *Optics Letters,* vol. 45, no. 6, pp. 1463-1466, 2020.

[12] H. Zhou *et al.*, "Photo detection and modulation from 1,550 to 2,000 nm realized by a GeSn/Ge multiple-quantum-well photodiode on a 300-mm Si substrate," *Optics Express,* vol. 28, no. 23, pp. 34772-34786, 2020.

[13] C. Chang, H. Li, S. Huang, H. Cheng, G. Sun, and R. J. A. P. L. Soref, "Sn-based Ge/Ge0. 975Sn0. 025/Ge pin photodetector

operated with back-side illumination," *J Applied Physics Letters,* vol. 108, no. 15, p. 151101, 2016.

[14] C. Chang *et al.*, "Ge 0.975 Sn 0.025 320× 256 imager chip for 1.6–1.9 μm infrared vision," *J Applied optics,* vol. 55, no. 36, pp. 10170-10173, 2016.

[15] H. Oka *et al.*, "Back-side illuminated GeSn photodiode array on quartz substrate fabricated by laser-induced liquid-phase crystallization for monolithically-integrated NIR imager chip," in *2017 IEEE International Electron Devices Meeting (IEDM)*, 2017, pp. 16.3. 1-16.3. 4: IEEE.

[16] S. Wu, L. Zhang, B. Son, Q. Chen, H. Zhou, and C. S. Tan, "Insights into the Origins of Guided Microtrenches and Microholes/rings from Sn Segregation in Germanium–Tin Epilayers," *The Journal of Physical Chemistry C,* vol. 124, no. 37, pp. 20035-20045, 2020.

[17] H. V. Stanchu *et al.*, "Strain suppressed Sn incorporation in GeSn epitaxially grown on Ge/Si (001) substrate," *Applied Physics Letters,* vol. 116, no. 23, p. 232101, 2020.

[18] J. Margetis *et al.*, "Study of low-defect and strain-relaxed GeSn growth via reduced pressure CVD in H2 and N2 carrier gas," *Journal of Crystal Growth,* vol. 463, pp. 128-133, 2017.

[19] D. Schmelz, M. Steglich, K. Dietrich, T. Käsebier, and U. D. Zeitner, "Black-silicon-structured back-illuminated Ge-on-Si photodiode arrays," in *Integrated Optics: Design, Devices, Systems, and Applications V*, 2019, vol. 11031, p. 1103109: International Society for Optics and Photonics.

[20] M. Steglich *et al.*, "Ge-on-Si photodiode with black silicon boosted responsivity," *J Applied Physics Letters,* vol. 107, no. 5, p. 051103, 2015.

[21] S. Xu *et al.*, "High-speed photo detection at two-micron-wavelength: technology enablement by GeSn/Ge multiple-quantum-well photodiode on 300 mm Si substrate," *Optics express,* vol. 27, no. 4, pp. 5798-5813, 2019.

[22] Y. Dong *et al.*, "Two-micron-wavelength germanium-tin photodiodes with low dark current and gigahertz bandwidth," *Optics Express,* vol. 25, no. 14, pp. 15818-15827, 2017.

[23] B. Son, Y. Lin, K. H. Lee, Y. Wang, S. Wu, and C. S. Tan, "High speed and ultra-low dark current Ge vertical pin photodetectors on an oxygen-annealed Ge-on-insulator platform with GeO x surface passivation," *Optics Express,* vol. 28, no. 16, pp. 23978-23990, 2020.

[24] Y. Dong *et al.*, "Suppression of dark current in germanium-tin on silicon pin photodiode by a silicon surface passivation technique," *Optics express,* vol. 23, no. 14, pp. 18611-18619, 2015.

[25] M. Morea *et al.*, "Passivation of multiple-quantum-well Ge0. 97Sn0. 03/Ge pin photodetectors," *Applied Physics Letters,* vol. 110, no. 9, p. 091109, 2017.

[26] Y.-F. Huang *et al.*, "Improved broadband and quasi-omnidirectional anti-reflection properties with biomimetic silicon nanostructures," *Nature nanotechnology,* vol. 2, no. 12, pp. 770-774, 2007.

[27] M. Steglich, T. Käsebier, M. Zilk, T. Pertsch, E.-B. Kley, and A. Tünnermann, "The structural and optical properties of black silicon by inductively coupled plasma reactive ion etching," *Journal of Applied Physics,* vol. 116, no. 17, p. 173503, 2014.

[28] Y. Yamada, H. Iizuka, and N. Mizoshita, "Silicon Nanocone Arrays via Pattern Transfer of Mushroomlike SiO2 Nanopillars for Broadband Antireflective Surfaces," *ACS Applied Nano Materials,* vol. 3, no. 5, pp. 4231-4240, 2020.

[29] M. Dai *et al.*, "Measurement of optical constants of TiN and TiN/Ti/TiN multilayer films for microwave kinetic inductance photon-number-resolving detectors," *Journal of Low Temperature Physics,* vol. 194, no. 5-6, pp. 361-369, 2019.

[30] S. Xu *et al.*, "Pseudomorphic GeSn/Ge Multiple-quantum-well on Silicon for Photo Detection and Modulation at 2 μm Wavelength Range," in *Optical Fiber Communication Conference*, 2019, p. Th2A. 10: Optical Society of America.

[31] T. Pham *et al.*, "Systematic study of Si-based GeSn photodiodes with 2.6 μm detector cutoff for short-wave infrared detection," *Optics express,* vol. 24, no. 5, pp. 4519-4531, 2016.

[32] M. Oehme, J. Werner, E. Kasper, M. Jutzi, and M. Berroth, "High bandwidth Ge p-i-n photodetector integrated on Si," *J Applied physics letters,* vol. 89, no. 7, p. 071117, 2006.